

Exploring Homogeneous and Heterogeneous Consistent Label Associations for Unsupervised Visible-Infrared Person ReID

Lingfeng He¹, De Cheng^{1*}, Nannan Wang¹, Xinbo Gao²,

¹ Xidian University, ² Chongqing University of Posts and Telecommunications

lfhe@stu.xidian.edu.cn, {dcheng, nnwang}@xidian.edu.cn

Abstract

Unsupervised visible-infrared person re-identification (USL-VI-ReID) aims to retrieve pedestrian images of the same identity from different modalities without annotations. While prior work focuses on establishing cross-modality pseudo-label associations to bridge the modality-gap, they ignore maintaining the instance-level homogeneous and heterogeneous consistency in pseudo-label space, resulting in coarse associations. In response, we introduce a Modality-Unified Label Transfer (MULT) module that simultaneously accounts for both homogeneous and heterogeneous fine-grained instance-level structures, yielding high-quality cross-modality label associations. It models both homogeneous and heterogeneous affinities, leveraging them to define the inconsistency for the pseudo-labels and then minimize it, leading to pseudo-labels that maintain alignment across modalities and consistency within intra-modality structures. Additionally, a straightforward plug-and-play Online Cross-memory Label Refinement (OCLR) module is proposed to further mitigate the impact of noisy pseudo-labels while simultaneously aligning different modalities, coupled with a Modality-Invariant Representation Learning (MIRL) framework. Experiments demonstrate that our proposed method outperforms existing USL-VI-ReID methods, highlighting the superiority of our MULT in comparison to other cross-modality association methods. The code will be available.

1. Introduction

Visible-infrared person re-identification (VI-ReID) [25, 44, 46, 49, 51, 56] aims at retrieving the same person from a set of visible/infrared gallery images when given an image from another modality. It has garnered growing interest due to its practical applications in intelligent surveillance systems. Existing VI-ReID methods have achieved remarkable performance with deep neural net-

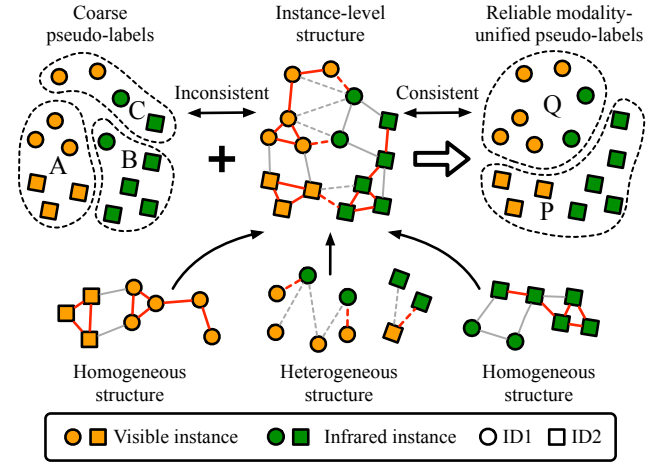


Figure 1. Illustration of our idea. Different colors denote different modalities, and different shapes denote different identities. The red lines represent higher affinities and the gray lines represent lower affinities. Our Modality-Unified Label Transfer takes into account instance-level structures to establish homogeneous and heterogeneous structurally consistent label associations and generate reliable modality-unified pseudo-labels for network training.

works [16, 19, 23, 28, 31, 35]. However, these works are based on datasets with modality-shared annotations, which are labor-intensive and time-consuming to obtain in real-world scenarios. To relieve such issues, we investigate the unsupervised solution for VI-ReID.

Although there are several unsupervised single-modality ReID methods that have achieved excellent performance (e.g., Cluster-Contrast [11], ISE [55], PPLR [8]), the direct application of these methods to VI-ReID scenarios presents a formidable challenge due to the substantial modality-gap. Images of the same pedestrian from different modalities cannot be assigned the same pseudo-label using conventional clustering-based methods. Therefore, associating cross-modality pseudo-labels is necessary for unsupervised VI-ReID. Several attempts [5, 6, 42, 46] have been made to associate the cross-modality pseudo-labels. PGM [46] and MBCCM [5] adopt a global perspective to inter-link cross-modality clusters. However, they overlook the

*Corresponding author

complicated, fine-grained structural information at the instance level, consequently resulting in coarse associations. To utilize the instance-level information, OTLA [42] formulates the label assignment between instance and cross-modality clusters as an Optimal Transport (OT) problem. Nevertheless, it neglects the homogeneous structural consistency, leading to intra-cluster instances in one modality being dispersed across multiple clusters in another modality. Based on the above analysis, we utilize instance-level pairwise relationships to establish reliable cross-modality label associations that maintain both homogeneous and heterogeneous structural consistency (as shown in Fig.1).

Specifically, we propose a Modality-Unified Label Transfer (MULT) module (Fig.2 (a)), which exploits the full potential of both homogeneous and heterogeneous instance-level structures to associate cross-modality pseudo-labels. To begin, our MULT excavates homogeneous and heterogeneous structural information by modeling affinities derived from pairwise instance relationships in feature space. These affinities are then utilized to define both homogeneous and heterogeneous inconsistency for pseudo-labels from a global perspective. Subsequently, MULT transfers the pseudo-labels guided by the calculated affinities, with the primary aim of minimizing the inconsistency terms. During the label transfer process, each instance communicates its pseudo-label information with both its intra-modality and cross-modality counterparts. Such transfer strategy leverages detailed instance-level relationships, facilitating more precise associations compared to the direct associations of clusters. Simultaneously, the pseudo-labels preserve the homogeneous structure in feature space by minimizing the homogeneous inconsistency terms. As a result, our MULT provides reliable supervision for training.

To achieve modality alignment based on pseudo-labels derived from MULT, we introduce an Online Cross-memory Label Refinement (OCLR) module (Fig.2 (c)), complemented by a Modality-Invariant Representation Learning (MIRL) framework (Fig.2 (b)). Specifically, our OCLR module is a straightforward yet effective plug-and-play component designed to alleviate the impact of the inevitable noisy pseudo-labels while further reducing the modality-gap. Specifically, it learns self-consistency among memory banks. Our MIRL framework conducts both intra-modality and cross-modality contrastive learning based on memory banks. Experimental results highlight the effectiveness of our OCLR, showcasing its applicability in various cross-modality label association methods.

Our main contributions can be summarized as follows:

- We propose a MULT module that considers instance-level context structures to provide homogeneous and heterogeneous structurally consistent cross-modality pseudo-label associations for network training.
- We design a straightforward plug-and-play OCLR mod-

ule for learning cross-memory self-consistency online, alleviating the impact of noisy labels while mitigating the modality-gap.

- Experiments on SYSU-MM01 and RegDB datasets demonstrate our method outperforms existing USL-VI-ReID methods, and our MULT generates higher-quality label associations than other methods.

2. Related Work

2.1. Unsupervised Single-Modality ReID

Unsupervised single-modality ReID aims to learn discriminative representations for unannotated person images. Recent unsupervised methods [11, 22, 26, 27, 41, 43, 52, 53, 55] follow a self-training pipeline that alternates between generating pseudo-labels and training the network. To alleviate the impact of noisy labels, MMT [14] utilize the Mean-Teacher [39] model to revise pseudo-labels online, while RLCC [54] and PPLR [8] generating offline soft pseudo-labels to refine hard labels. SPCL [15], Cluster-Contrast [11] and ISE [55] propose constructing memory banks, which store unique prototypes for unlabeled clusters.

Following the memory-based methods, we construct intra-modality and cross-modality memory banks to perform contrastive learning for heterogeneous features.

2.2. Unsupervised VI-ReID

Unsupervised VI-ReID aims to learn modality-invariant and identity-discriminative features for cross-modality images without annotations. Existing methods [5, 6, 24, 46, 47] mainly focus on associating cross-modality pseudo-labels. H2H [24] and ADCA [47] associate heterogeneous instances from a local perspective according to pairwise similarities. To avoid biased label associations, OTLA [42] establishes an optimal transport problem to assign cross-modality pseudo-labels uniformly for instances. To model the cross-modality relationships from a global perspective, PGM [46] and MBCCM [5] construct bipartite graphs to match cross-modality clusters. Furthermore, GRU [48] proposes a CAE module to embed the information of hierarchical domains while achieving remarkable performance.

In contrast to the above-mentioned methods, our MULT simultaneously utilizes the homogeneous and heterogeneous instance-level structures to provide reliable cross-modality label associations.

2.3. Affinity-Based Person ReID

In the person ReID task, some works [2, 23, 29, 30, 36, 37, 49] pay attention to the detailed relationships between pairwise instances. SSFT [30] proposes a feature transfer module to facilitate the optimization of group-wise similarities for single-modality ReID. cm-SSFT [29] models both intra-modality and cross-modality affinities to generate

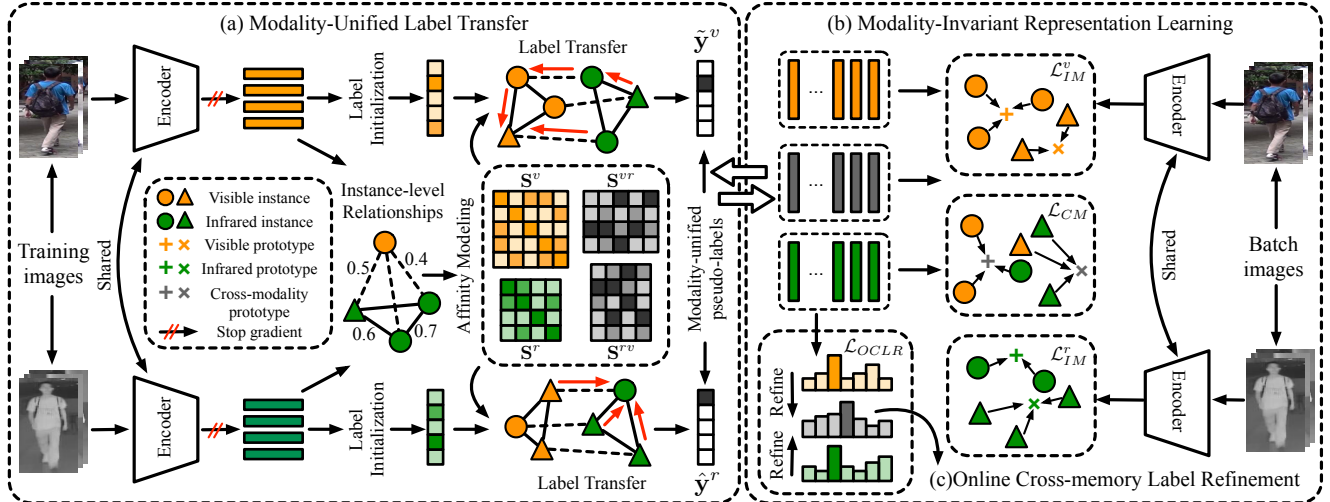


Figure 2. Framework of our proposed method. Different colors indicate different modalities. Our method alternates pseudo-label generation (Modality-Unified Label Transfer (MULT (a), described in Sec.3.1)) and network training (including Modality-Invariant Representation Learning (MIRL (b), described in Sec.3.2) and Online Cross-memory Label Refinement (OCLR (c), described in Sec.3.3)).

modality-shared features from modality-specific features. CIFT [23] proposes a novel graph module to simulate the unbalanced modality distribution.

Inspired by the widely-used GCN [21] and the above affinity-based methods, we model affinities in feature space to fully exploit instance-level relationships.

3. Methodology

Given a visible-infrared dataset $\mathcal{X} = \{\mathcal{X}^v, \mathcal{X}^r\}$, $\mathcal{X}^v = \{\mathbf{x}_i^v | i = 1, 2, \dots, N^v\}$ and $\mathcal{X}^r = \{\mathbf{x}_i^r | i = 1, 2, \dots, N^r\}$ represents the visible and infrared datasets with N^v and N^r images, respectively. In the context of the USL-VI-ReID task, our objective is to train a deep neural network $f_\theta(\cdot)$ to project an image \mathbf{x}_i from the dataset \mathcal{X} into an embedding space \mathcal{F}_θ and derive a d-dimensional modality-invariant representation $\mathbf{f}_i = f_\theta(\mathbf{x}_i) \in \mathbb{R}^d$.

We employ the two stream encoder $f_\theta(\cdot)$ (e.g., ResNet50 [17]) to extract visible features $\{\mathbf{f}_i^v | i = 1, 2, \dots, N^v\}$ and infrared features $\{\mathbf{f}_i^r | i = 1, 2, \dots, N^r\}$. In the initial training stage, following [5, 46, 47], we employ the Dual-Contrastive Learning (DCL) framework [47] to facilitate intra-modality contrastive learning as our baseline.

Our proposed method is employed during the second training stage. The framework is illustrated in Fig.2. Following the well-developed unsupervised methods [11, 15, 47, 55], we alternate between pseudo-label generation and network training. During the pseudo-label generation stage, following [5, 46, 47], we first utilize DBSCAN [13] to cluster features. Two intra-modality memory banks $\hat{\mathbf{M}}^v \in \mathbb{R}^{K^v \times d}$ and $\hat{\mathbf{M}}^r \in \mathbb{R}^{K^r \times d}$ are initialized by the cluster centroids of their corresponding modalities, where K^v and K^r denotes the number of clusters in the visible modality and the infrared modality, respectively. Then the proposed

Modality-Unified Label Transfer (MULT, Fig.2 (a)) establishes reliable cross-modality label associations for network training. During the training stage, we perform Modality-Invariant Representation learning (MIRL, Fig.2 (b)) to fully leverage the supervisory signals from MULT. Additionally, an Online Cross-memory Label refinement (OCLR, Fig.2 (c)) module is proposed to further alleviate the influence of noisy labels. Our entire framework includes two training modes, i.e., V-based and R-based, where V-based denotes we utilize pseudo-labels in the visible label space to guide network training, and vice versa. Following PGM [46], we alternate these two modes during training. For convenience, we only explain the V-based training mode below.

3.1. Modality-Unified Label Transfer

Motivated by the affinity-based ReID methods [23, 29, 30], Our MULT models instance-wise affinities to generate structurally consistent pseudo-labels. In MULT, every instance holds two types of pseudo-labels, i.e., the intra-modality label (labels from the label space corresponding to the instance’s modality) and the cross-modality label (labels from the label space corresponding to another modality). We use $\mathbf{y}^e = \{\hat{\mathbf{y}}^e, \hat{\mathbf{y}}^e\}$ to denote the pseudo-labels, where $\hat{\mathbf{y}}^e$ denotes the intra-modality labels and $\hat{\mathbf{y}}^e$ denotes the cross-modality labels ($e = \{v, r\}$ indicates visible and infrared modality, respectively), and \mathbf{y}_i^e denotes the pseudo-label of i -th instance in modality e . Our MULT includes two directions, i.e., V2R and R2V. We only describe the V2R MULT, which involves the transfer between visible intra-modality labels $\hat{\mathbf{y}}^v$ and infrared cross-modality labels $\hat{\mathbf{y}}^r$.

Label Initialization. To fully utilize the relationships between instances and each cluster centroid, we use the soft probability distribution from the corresponding mem-

ory bank as initial visible intra-modality labels $\tilde{\mathbf{y}}^v$:

$$\tilde{\mathbf{y}}^v \in \mathbb{R}^{N^v \times K^v}, \tilde{\mathbf{y}}_i^v(0) = \mathbf{P}(\mathbf{f}_i^v | \tilde{\mathbf{M}}^v, \tau) \in \mathbb{R}^{K^v}, \quad (1)$$

where $\mathbf{P}(\mathbf{f} | \mathbf{M}, \tau)$ denotes the probability distribution output from memory bank \mathbf{M} for feature \mathbf{f} with the temperature factor τ , which can be formulated as:

$$P_j(\mathbf{f} | \mathbf{M}, \tau) = \frac{\exp(\mathbf{f}^\top \mathbf{c}_j / \tau)}{\sum_{k=1}^K \exp(\mathbf{f}^\top \mathbf{c}_k / \tau)}, \quad (2)$$

$$\mathbf{P}(\mathbf{f} | \mathbf{M}, \tau) = [P_1(\mathbf{f} | \mathbf{M}, \tau), \dots, P_K(\mathbf{f} | \mathbf{M}, \tau)], \quad (3)$$

where K denotes the number of prototypes in \mathbf{M} . Following [6, 42], we utilize Optimal Transport Label Assignment (OTLA) to initialize infrared cross-modality labels $\hat{\mathbf{y}}^r$:

$$\hat{\mathbf{y}}^r(0) = OTLA(\mathbf{f}^r, \tilde{\mathbf{M}}^v) \in \mathbb{R}^{N^r \times K^v}, \quad (4)$$

where $OTLA(\mathbf{f}^r, \tilde{\mathbf{M}}^v)$ indicates formulating the assignment of pseudo-labels in visible modality to instances in infrared modality as the OT problem, where the cost matrix for OT is calculated by \mathbf{f}^r and $\tilde{\mathbf{M}}^v$.

Affinity Modeling. To incorporate instance-level relationships, we model the homogeneous and heterogeneous affinities, denoted as $\mathbf{S}^{ho(e)}$ and \mathbf{S}^{he} . Note that $\mathbf{S}^{ho(e)} = \{\mathbf{S}^{ho(v)}, \mathbf{S}^{ho(r)}\}$ denotes the affinities within visible and infrared modalities, respectively. To enhance the utilization of contextual information, we employ the *Jaccard Similarity* to model *the homogeneous affinities*:

$$\mathbf{S}^{ho(e)} \in \mathbb{R}^{N^e \times N^e}, \mathbf{S}_{ij}^{ho(e)} = \frac{|\mathcal{R}(\mathbf{f}_i^e, \kappa) \cap \mathcal{R}(\mathbf{f}_j^e, \kappa)|}{|\mathcal{R}(\mathbf{f}_i^e, \kappa) \cup \mathcal{R}(\mathbf{f}_j^e, \kappa)|}, \quad (5)$$

where $N^e = \{N^v, N^r\}$ denotes the number of instances in modality $e = \{v, r\}$. $\mathbf{S}_{ij}^{ho(e)}$ can be regarded as the affinity between \mathbf{f}_i^e and \mathbf{f}_j^e in modality e , and $\mathcal{R}(\mathbf{f}_i^e, \kappa)$ is the κ -reciprocal nearest neighbors [57] of \mathbf{f}_i^e .

Due to the substantial modality discrepancy, directly modeling the heterogeneous affinity by the *Jaccard Similarities* between cross-modality features as Eq.5 to model the heterogeneous affinity will lead to the problem of modality-bias: some instances are naturally closer to another modality so they hold a higher degree of total affinity to that modality. To address the modality-bias, we hope all instances within one modality have an equal total affinity to another modality. Thus we model *the heterogeneous affinities* by solving the Optimal Transport (OT) plan according to the transport cost between cross-modality features, which can be formulated as:

$$\begin{aligned} & \min_{\mathbf{S}^{he}} \langle \mathbf{S}^{he}, \mathbf{C}^{he} \rangle + \frac{1}{\lambda} \langle \mathbf{S}^{he}, -\log(\mathbf{S}^{he}) \rangle. \\ \text{s.t. } & \mathbf{S}^{he} \mathbf{1} = \mathbf{1} \cdot \frac{1}{N^v}, \mathbf{S}^{he \top} \mathbf{1} = \mathbf{1} \cdot \frac{1}{N^r}, \end{aligned} \quad (6)$$

where $\mathbf{S}^{he} \in \mathbb{R}^{N^v \times N^r}$ denotes the transport plan. $\mathbf{C}^{he} \in \mathbb{R}^{N^v \times N^r}$ is the cost matrix constructed by computing the Euclidean distance of heterogeneous features, i.e., $\mathbf{C}_{ij}^{he} = \|\mathbf{f}_i^v - \mathbf{f}_j^r\|_2^2$. $\langle \cdot \rangle$ denotes the Frobenius dot-product, λ is a hyper-parameter and $\mathbf{1}$ is an all in 1 vector. The first term in the objective function in Eq.6 indicates the total transport cost and the second term is the Entropic Regularization [9]. The constraints ensure each instance in the visible (infrared) modality holds an equal total affinity to instances in the infrared (visible) modality. The optimal solution \mathbf{S}^{he*} of Eq.6 can be obtained by the Sinkhorn-Knopp algorithm [10] and \mathbf{S}_{ij}^{he*} can be regarded as the affinity between heterogeneous features \mathbf{f}_i^v and \mathbf{f}_j^r .

We then derive the visible-to-infrared affinity matrix $\mathbf{S}^{he(vr)} = \mathbf{S}^{he*} \in \mathbb{R}^{N^v \times N^r}$ and the infrared-to-visible affinity matrix $\mathbf{S}^{he(rv)} = \mathbf{S}^{he* \top} \in \mathbb{R}^{N^r \times N^v}$ from the heterogeneous affinities \mathbf{S}^{he*} . We perform row normalization on the above affinities and obtain the final affinity matrices $\mathbf{S} = \{\mathbf{S}^{ho(v)}, \mathbf{S}^{ho(r)}, \mathbf{S}^{he(vr)}, \mathbf{S}^{he(rv)}\}$, which are subsequently employed to define the structural inconsistency.

Inconsistency Formulation. We leverage the above affinities to define the inconsistency terms for pseudo-labels. A minor degree of structural inconsistency implies that the higher the affinity between two instances, the smaller the distance between their pseudo-labels. Consequently, we define the product of the Euclidean distance between pseudo-labels of pairwise instances and their affinity as their structural inconsistency. From a global perspective, for all instances in both modalities, *the homogenous inconsistency* can be formulated as follows:

$$\mathcal{I}_{ho}(\mathbf{y}^e) = \sum_{i=1}^{N^e} \sum_{j=1}^{N^e} \mathbf{S}_{ij}^{ho(e)} \|\mathbf{y}_i^e - \mathbf{y}_j^e\|_2^2. \quad (7)$$

Here $\mathbf{y}^e = \{\tilde{\mathbf{y}}^v, \hat{\mathbf{y}}^r\}$ denotes the pseudo-labels involved in the process of V2R MULT. *The heterogeneous inconsistency* can be formulated in a similar manner:

$$\begin{aligned} \mathcal{I}_{he}^v(\tilde{\mathbf{y}}^v) &= \sum_{i=1}^{N^v} \sum_{j=1}^{N^r} \mathbf{S}_{ij}^{he(vr)} \|\tilde{\mathbf{y}}_i^v - \hat{\mathbf{y}}_j^r\|_2^2, \\ \mathcal{I}_{he}^r(\hat{\mathbf{y}}^r) &= \sum_{i=1}^{N^r} \sum_{j=1}^{N^v} \mathbf{S}_{ij}^{he(rv)} \|\hat{\mathbf{y}}_i^r - \tilde{\mathbf{y}}_j^v\|_2^2. \end{aligned} \quad (8)$$

Nonetheless, solely minimizing the above two inconsistency terms can lead to a collapse, where all instances end up with nearly identical labels. This is because these two inconsistency statements do not consider the fact that pairwise instances with low affinities should have distinct labels. To avoid such collapse, we propose *the self-inconsistency* to constraint the Euclidean distance between the transferred labels and the initial coarse labels:

$$\mathcal{I}_{self}^e(\mathbf{y}^e) = \sum_{i=1}^{N^e} \|\mathbf{y}_i^e - \mathbf{y}_i^e(0)\|_2^2. \quad (9)$$

We minimize the above three terms of inconsistency, aiming to derive the pseudo-labels \mathbf{y}^e with the lowest inconsistency. This optimization can be formulated as follows:

$$\min_{\mathbf{y}^e} \mathcal{I}_{ho}^e(\mathbf{y}^e) + \alpha \mathcal{I}_{self}^e(\mathbf{y}^e) + (1 - \alpha) \mathcal{I}_{he}^e(\mathbf{y}^e), \quad (10)$$

where α is a trade-off parameter.

Label Transfer. The above optimization problem can be solved by the LGC algorithm [58]. Specifically, the visible and infrared modality-unified labels are updated alternately as Eq.11 and Eq.12 until convergence:

$$\begin{aligned} \tilde{\mathbf{y}}^v(t+1) &= (1 - \alpha) \mathbf{S}^{he(vr)} \cdot \hat{\mathbf{y}}^r(t) + \alpha \tilde{\mathbf{y}}^v(0), \\ \tilde{\mathbf{y}}^v(t+1) &= \frac{1}{2} (\mathbf{S}^{ho(v)} \cdot \tilde{\mathbf{y}}^v(t+1) + \tilde{\mathbf{y}}^v(t+1)), \end{aligned} \quad (11)$$

$$\begin{aligned} \hat{\mathbf{y}}^r(t+1) &= (1 - \alpha) \mathbf{S}^{he(rv)} \cdot \tilde{\mathbf{y}}^v(t) + \alpha \hat{\mathbf{y}}^r(0), \\ \hat{\mathbf{y}}^r(t+1) &= \frac{1}{2} (\mathbf{S}^{ho(r)} \cdot \hat{\mathbf{y}}^r(t+1) + \hat{\mathbf{y}}^r(t+1)), \end{aligned} \quad (12)$$

where $\mathbf{y}^e(t) = \{\tilde{\mathbf{y}}^v(t), \hat{\mathbf{y}}^r(t)\}$ denotes the labels in t -th iteration during the optimization process.

Nevertheless, the transferred pseudo-labels are excessively smoothed, which is detrimental to the network's ability to learn predictions with low entropy. Therefore, we derive the soft modality-unified labels by aggregating both hard labels and soft labels, which can be formulated as:

$$\mathbf{y}^e = \beta \cdot \mathbf{y}_{hard}^e + (1 - \beta) \cdot \mathbf{y}_{soft}^e, \quad (13)$$

where \mathbf{y}_{hard} and \mathbf{y}_{soft} denotes the hard pseudo-labels and the soft pseudo-labels obtained from the transferred labels $\mathbf{y}^e = \{\tilde{\mathbf{y}}^v, \hat{\mathbf{y}}^r\}$, respectively. β is a parameter to control the smoothness of the pseudo-label. It is noteworthy that the labels $\tilde{\mathbf{y}}_i^v$ and $\hat{\mathbf{y}}_i^r$ have a same dimension of K .

3.2. Modality-Invariant Representation Learning

Guided by the modality-unified soft labels from the MULT module, we lay emphasis on alleviating the cross-modality discrepancy while keeping intra-modality consistency. Following the MSMA framework [5], we concurrently execute intra-modality and cross-modality contrastive learning. To be specific, we construct a cross-modality memory bank $\mathbf{M}^a \in \mathbb{R}^{K^v \times d}$ and an intra-cross-modality memory bank $\tilde{\mathbf{M}}^r \in \mathbb{R}^{K^v \times d}$, which are initialized in the same manner as the visible intra-modality memory bank $\tilde{\mathbf{M}}^v$. Following the widely-used memory-based methods [7, 11, 15, 47], we carry out contrastive learning during forward-propagation (FP) and update the memory banks during backward-propagation (BP). The visible intra-modality contrastive loss can be formulated as:

$$\mathcal{L}_{IM}^v = \frac{1}{B} \sum_{i=1}^B \mathcal{L}_{ce}(\mathbf{P}(\mathbf{f}_i^v | \tilde{\mathbf{M}}^v, \tau), \tilde{\mathbf{y}}_i^v), \quad (14)$$

where \mathcal{L}_{ce} denotes the standard cross-entropy loss. For infrared modality, every instance owns two types of labels, i.e., $\tilde{\mathbf{y}}^r$ and $\hat{\mathbf{y}}^r$. Such two types of labels are utilized jointly for infrared intra-modality contrastive learning, which can be formulated as:

$$\begin{aligned} \mathcal{L}_{IM}^r &= \frac{1}{B} \sum_{i=1}^B \mathcal{L}_{ce}(\mathbf{P}(\mathbf{f}_i^r | \tilde{\mathbf{M}}^r, \tau), \tilde{\mathbf{y}}_i^r) \\ &+ \frac{1}{B} \sum_{i=1}^B \mathcal{L}_{ce}(\mathbf{P}(\mathbf{f}_i^r | \hat{\mathbf{M}}^r, \tau), \hat{\mathbf{y}}_i^r). \end{aligned} \quad (15)$$

These two types of labels play a mutual corrective role and facilitate intra-modality training. The total intra-modality contrastive loss can be formulated as follows:

$$\mathcal{L}_{IM} = \mathcal{L}_{IM}^v + \mathcal{L}_{IM}^r. \quad (16)$$

Besides, we perform cross-modality contrastive learning to learn modality-invariant representations:

$$\begin{aligned} \mathcal{L}_{CM} &= \frac{1}{B} \sum_{i=1}^B \mathcal{L}_{ce}(\mathbf{P}(\mathbf{f}_i^v | \mathbf{M}^a, \tau), \tilde{\mathbf{y}}_i^v) \\ &+ \frac{1}{B} \sum_{i=1}^B \mathcal{L}_{ce}(\mathbf{P}(\mathbf{f}_i^r | \mathbf{M}^a, \tau), \hat{\mathbf{y}}_i^r). \end{aligned} \quad (17)$$

During the BP stage, the memory banks are updated with the input features in a momentum strategy [11, 18]:

$$\mathbf{m}(y_i^e) \leftarrow \mu \mathbf{m}(y_i^e) + (1 - \mu) \mathbf{f}(y_i^e), \quad (18)$$

where μ is the momentum updating factor. $\mathbf{m}(y_i^e)$ is the y_i^e -th prototype in the memory bank \mathbf{M} , and $\mathbf{f}(y_i^e)$ is the input feature with label y_i^e in current mini-batch. Note that the hard label y_i^e for memory update is derived from the soft modality-unified label y_i^e .

3.3. Online Cross-memory Label Refinement

While the MULT module enables training under modality-unified supervision, it is essential to consider that due to the inherent noise in clustering and MULT, prolonged training with fixed supervised signals may cause the network to overfit incorrect labels.

To overcome this issue, we utilize the predictions from the intra-modality memory banks to refine the predictions from the cross-modality memory bank. Several reasons support the adoption of such refinement strategies: (1) The intra-modality memory banks are updated by features within their respective modalities, this update occurs at a slower rate compared to the cross-modality memory bank, resulting in more stable predictions. (2) The intra-modality

Table 1. Comparison with the state-of-the-art methods on SYSU-MM01 and RegDB. ‘GUR*’ denotes GUR without camera labels. Since our method does not require any camera label information, for fair comparison we do not report the results of GUR with camera labels.

Method	Venue	SYSU-MM01						RegDB					
		All-search			Indoor-search			Visible-to-Infrared			Visible-to-Infrared		
		R1	mAP	mINP	R1	mAP	mINP	R1	mAP	mINP	R1	mAP	mINP
<i>Supervised VI-ReID methods</i>													
AGW [51]	TPAMI-21	47.50	47.65	35.30	54.17	62.97	59.23	70.05	66.37	50.19	70.49	65.90	51.24
VCD+VML [40]	CVPR-21	60.02	58.80	-	66.05	72.98	-	73.2	71.6	-	71.8	70.1	-
MPANet [45]	CVPR-21	70.58	68.24	-	76.74	80.95	-	82.8	80.7	-	83.7	80.9	-
MAUM [28]	CVPR-22	71.68	68.79	-	76.97	81.94	-	87.87	85.09	-	86.95	84.34	-
CIFT [23]	ECCV-22	74.08	74.79	-	81.82	85.61	-	91.96	92.00	-	90.30	90.78	-
SEFEL [20]	CVPR-23	77.12	72.33	-	82.07	82.95	-	91.07	85.23	-	92.18	86.59	-
PartMix [20]	CVPR-23	77.78	74.62	-	81.52	84.38	-	84.93	82.52	-	85.66	82.27	-
<i>Unsupervised single-modality ReID methods</i>													
MMT [14]	ICLR-20	21.47	21.53	11.50	22.79	31.50	27.66	25.68	26.51	19.56	24.42	25.59	18.66
Cluster-Contrast [11]	arXiv-21	20.16	22.00	12.97	23.33	34.01	30.88	11.76	13.88	9.94	11.14	12.99	8.99
ICE [3]	ICCV-21	20.54	20.39	10.24	29.81	38.35	34.32	12.98	15.64	11.91	12.18	14.82	10.6
PPLR [8]	CVPR-22	11.98	12.25	4.97	12.71	20.81	17.61	10.30	11.94	8.10	10.39	11.23	7.04
<i>Unsupervised VI-ReID methods</i>													
H2H [24]	TIP-21	25.49	25.16	-	-	-	-	13.91	12.72	-	14.11	2.29	-
H2H(AGW) [24]	TIP-21	30.15	29.40	-	-	-	-	23.81	18.87	-	-	-	-
H2H(AGW) w/ CMRR [24]	TIP-21	45.47	47.99	-	-	-	-	35.18	36.46	-	-	-	-
OTLA [42]	ECCV-22	29.9	27.1	-	29.8	38.8	-	32.9	29.7	-	32.1	28.6	-
ADCA [47]	MM-22	45.51	42.73	28.29	50.60	59.11	55.17	67.20	64.05	52.67	68.48	63.81	49.62
ADCA(AGW) [47]	MM-22	50.90	45.70	29.12	51.39	59.82	56.08	66.62	63.47	-	67.29	62.98	-
CHCR (AGW) [34]	T-CSVT-23	47.72	45.34	-	-	-	-	68.18	63.75	-	69.96	65.87	-
DOTLA (AGW) [6]	MM-23	50.36	47.36	32.40	53.47	61.73	57.35	85.63	76.71	61.58	82.91	74.97	58.60
MBCCM [5]	MM-23	53.14	48.16	32.41	55.21	61.98	57.23	83.79	77.87	65.04	82.82	76.74	61.73
CCLNet (CLIP) [4]	MM-23	54.03	50.19	-	56.68	65.12	-	69.94	65.53	-	70.17	66.66	-
PGM(AGW) [46]	CVPR-23	57.27	51.78	34.96	56.23	62.74	58.13	69.48	65.41	-	69.85	65.17	-
GUR* [48]	ICCV-23	60.95	56.99	41.85	64.22	69.49	64.81	73.91	70.23	58.88	75.00	69.94	56.21
Ours	-	65.03	58.62	42.77	65.35	71.24	66.60	91.50	83.73	69.13	89.08	80.88	64.03
Ours w/ CMRR [24]	Ours + TIP-21	71.39	67.68	55.48	69.75	74.53	70.16	92.77	93.86	93.04	90.34	91.91	91.18

and cross-modality memory banks are expected to output consistent predictions. The OCLR loss for visible modality can be formulated as follows:

$$\begin{aligned} \mathcal{L}_{OCLR}^v &= \frac{1}{B} \sum_{i=1}^B \mathcal{L}_{ce}(\mathbf{P}(\mathbf{f}_i^v | \mathbf{M}^a, \tau), P(\mathbf{f}_i^v | \tilde{\mathbf{M}}^v, \frac{1}{5}\tau)) \\ &+ \frac{1}{B} \sum_{i=1}^B \mathcal{L}_{ce}(\mathbf{P}(\mathbf{f}_i^v | \mathbf{M}^a, \tau), \mathbf{P}(\mathbf{f}_i^v | \hat{\mathbf{M}}^r, \frac{1}{5}\tau)). \end{aligned} \quad (19)$$

As in [1, 32], we sharpen the target prediction more than the source’s to encourage entropy minimization. The setting of the sharpen ratio follows ProtoCon [32]. In the visible modality, our OCLR operated between the visible stream and the augmented stream [47], enhancing constraints on self-consistency. The OCLR loss for infrared modality \mathcal{L}_{OCLR}^r can be formulated similarly.

3.4. Optimization

The total training loss can be formulated as follows:

$$\mathcal{L} = \mathcal{L}_{IM} + \mathcal{L}_{CM} + \mathcal{L}_{OCLR}^v + \mathcal{L}_{OCLR}^r, \quad (20)$$

where \mathcal{L}_{IM} , \mathcal{L}_{CM} , \mathcal{L}_{OCLR}^v and \mathcal{L}_{OCLR}^r are described in detail in Sec.3.2 and Sec.3.3. The training process is summarized in the supplementary material.

4. Experiments

4.1. Dataset and Evaluation Protocol

Datasets. Our proposed method is evaluated on two public visible-infrared datasets, namely SYSU-MM01 [44] and RegDB [33]. SYSU-MM01 comprises 395 identities, with 22258 visible and 11909 infrared images captured by indoor and outdoor cameras. RegDB is a smaller dataset obtained from a pair of aligned visible and infrared cameras [33]. It contains 412 identities, where each identity has 10 visible images and 10 infrared images.

Evaluation Metrics. All experiments follow the common evaluation protocols used for VI-ReID [49–51]. The evaluation metrics include Cumulative Matching Characteristic (CMC), Mean Average Precision (mAP), and Mean Inverse Negative Penalty (mINP [51]). For the SYSU-MM01 dataset, we evaluate the proposed method under two search modes: the All-search mode and the Indoor-search mode. As for the RegDB dataset, we evaluate our method on two testing modes: Visible-to-Infrared and Infrared-to-Visible. We randomly selected 206 identities for training and the remaining 206 for testing.

Implementation Details. Our proposed method is implemented using PyTorch. we adopt two-stream ResNet50 [17] pretrained on ImageNet [12] as our backbone. In a mini-batch, the number of classes P and instances for each class K are both 12. All the input images are resized to

Table 2. Ablation study on individual components of our method on SYSU-MM01 and RegDB.

Index	Method	SYSU-MM01						RegDB					
		All-search			Indoor-search			Visible-to-Infrared			Visible-to-Infrared		
		R1	mAP	mINP	R1	mAP	mINP	R1	mAP	mINP	R1	mAP	mINP
1	Baseline	41.76	38.57	24.32	45.83	54.44	50.00	50.58	48.78	35.62	51.17	47.24	33.80
<i>The following methods are all based on the MULT module</i>													
2	Baseline + \mathcal{L}_{CM}	60.43	53.98	37.28	58.79	64.61	59.29	76.31	67.97	50.62	78.11	66.55	45.64
3	Baseline + $\mathcal{L}_{IM} + \mathcal{L}_{CM}$	61.48	54.43	38.02	60.73	66.32	61.52	76.21	67.94	51.40	74.95	65.34	45.46
4	Baseline + \mathcal{L}_{OCLR}	51.88	47.37	31.39	52.63	59.44	55.29	86.80	80.36	66.44	86.84	79.29	61.36
5	Baseline + $\mathcal{L}_{IM} + \mathcal{L}_{OCLR}$	61.43	56.08	40.59	64.67	70.43	66.46	88.59	82.18	68.84	88.01	80.57	64.22
6	Baseline + $\mathcal{L}_{CM} + \mathcal{L}_{OCLR}$	61.16	56.21	40.92	62.18	68.31	63.94	88.64	82.05	68.85	87.62	80.82	65.26
7	Baseline + $\mathcal{L}_{IM} + \mathcal{L}_{CM} + \mathcal{L}_{OCLR}$	65.03	58.62	42.77	65.35	71.24	66.60	91.50	83.73	69.13	89.08	80.88	64.03

Table 3. Comparison with other cross-modality label association methods for unsupervised VI-ReID on SYSU-MM01. All experiments are based on our MIRL framework (Sec.3.2).

Method	All-search			Indoor-search	
	R1	mAP	mINP	R1	mAP
Baseline	41.76	38.57	24.32	45.83	54.43
<i>MIRL (Sec.3.2) w/o OCLR (Sec.3.3)</i>					
w/ PGM [46]	48.30	43.09	27.67	45.65	53.73
w/ BCCM [5]	53.80	47.55	30.53	50.72	59.41
w/ DOTLA [6]	59.27	50.60	32.36	55.34	62.76
w/ MULT (Ours)	61.48	54.43	38.02	60.73	66.32
<i>MIRL (Sec.3.2) w/ OCLR (Sec.3.3)</i>					
w/ PGM [46]	54.54	49.88	34.01	54.94	62.98
w/ BCCM [5]	55.64	50.69	34.79	57.80	65.47
w/ DOTLA [6]	61.74	54.65	38.61	59.19	66.84
w/ MULT (Ours)	65.03	58.62	42.77	65.35	71.24

288 × 144. The augmentations for images are following [47]. Besides, Linear Transform Generator (LTG [38]) and ColorJitter augmentations are adopted in the DCL training stage. We train for a total of 90 epochs. The DCL framework is trained in the first 40 epochs, while our proposed framework is trained in the other 50 epochs. We use the Adam optimizer for training the model with weight decay 5e-4. The initial learning rate is set to 3.5e-4 and decays 10 times at the 20th, 60th, and 80th epochs. Following [5, 46, 47], the momentum factor μ is 0.1, and the temperature τ is 0.05, while the maximum distance for DBSCAN is set to 0.6 on SYSU-MM01 and 0.3 on RegDB. The parameter κ for κ -reciprocal nearest neighbors in Eq.5 is set to 30 following [57]. The hyper-parameter λ in Eq.6 for OT is set to 25 following [42]. The trade-off parameter α in Eq.10 is set to 0.2 and β in Eq.13 is set to 0.7.

4.2. Comparison with State-of-the-Arts

To demonstrate the efficiency of our proposed methods, we compare our method with state-of-the-art methods under three relevant settings on SYSU-MM01 and RegDB datasets, i.e., supervised VI-ReID methods, unsupervised single-modality ReID methods, and unsupervised VI-ReID methods. The results are shown in Tab.1.

Comparison with Supervised VI-ReID Methods. Our proposed method achieves competitive performance with supervised method VCD+VML [40] on SYSU-MM01, while demonstrating excellent performance close to the state-of-the-art supervised methods on RegDB.

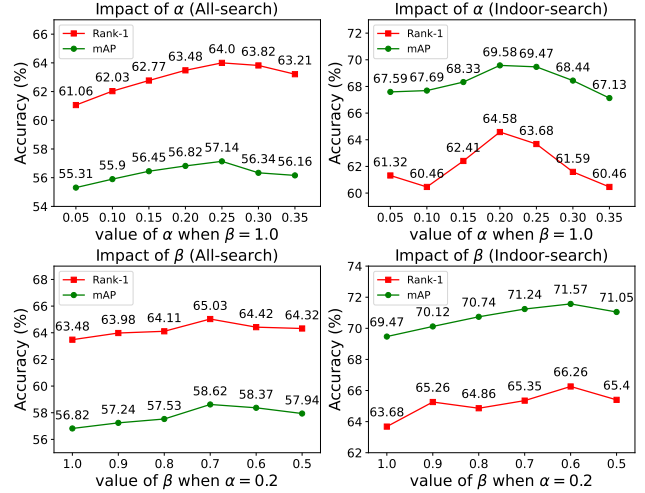


Figure 3. Parameter analysis of α and β on SYSU-MM01.

Comparison with Conventional Unsupervised Single-Modality ReID Methods. The results in Tab.1 indicate that unsupervised single-modality methods cannot effectively address the large modality-gap in cross-modality scenarios, emphasizing the necessity of proposing cross-modality label association strategies for VI-ReID.

Comparison with Unsupervised VI-ReID Methods. As reported in Tab.1, our method outperform the state-of-the-art GRU [48] by 1.63% mAP, 4.08% Rank-1 on SYSU-MM01 (All-search) and 13.5% mAP, 17.59% Rank-1 on RegDB (Visible-to-infrared). The proposed method has three main advantages: (1) Unlike H2H [24] and OTLA [42], our method does not require additional datasets or camera labels for training. (2) Our MULT associates cross-modality labels from a novel perspective and can be applied to other unsupervised cross-domain tasks. (3) Our OCLR is a plug-and-play module that can be employed in other unsupervised memory-based methods to handle label noise.

4.3. Ablation Study

To validate the effectiveness of each component of our method, we conduct ablation experiments on SYSU-MM01 and RegDB datasets, as shown in Tab.2. Our baseline consists of a two-stream ResNet trained under the DCL framework [47]. All experiments are conducted with our MULT module. We did not perform an ablation study on \mathcal{L}_{IM} as it

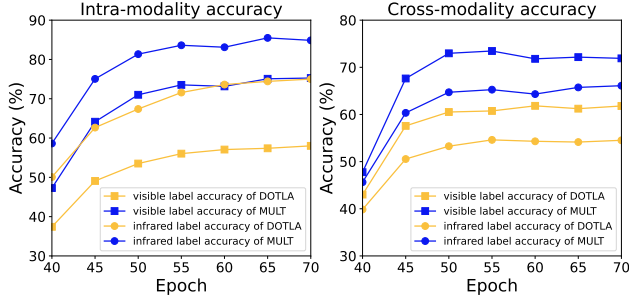


Figure 4. Accuracy of intra-modality and cross-modality positive pairs found by pseudo-labels on SYSU-MM01.

does not address the problem of modality discrepancy.

Effectiveness of MULT. The MULT module delivers a +15.41% mAP and +18.67% Rank-1 improvement by directly incorporating \mathcal{L}_{CM} (see 1st row and 2nd row in Tab.2) and achieves +20.05% mAP and +23.27% Rank-1 improvement when trained within our entire framework on SYSU-MM01 (see 1st row and 7th row in Tab.2). To further evaluate the effectiveness of MULT, we compare MULT with other cross-modality label association methods in Tab.3, including PGM [46], MBCCM [5] and DOTLA [6]. The results demonstrate our MULT provides higher-quality associations than other methods.

Effectiveness of OCLR. The OCLR module provides a performance gain of +8.8% mAP and +10.12% Rank-1 when directly adding it to our baseline (see 1st row and 4th row in Tab.2). When used in conjunction with our MIRL framework, the OCLR further improves the performance of +4.19% mAP and +3.55% Rank-1 (see 3rd row and 7th row in Tab.2). OCLR utilizes ever-evolving prototypes for online refinement, avoiding overfitting noisy labels. We also integrate our OCLR into other methods (see upper and lower in Tab.3) based on our MIRL framework. The results indicate that our OCLR improves performance when collaborating with other cross-modality association methods.

Effectiveness of MIRL. Our MIRL achieves +0.45% mAP improvement without OCLR (see 2nd row and 3rd row in Tab.2) and achieves +2.41% mAP with OCLR (see 6th row and 7th row in Tab.2) compared to leveraging \mathcal{L}_{CM} alone. The results illustrate the importance of incorporating intra-modality contrastive loss \mathcal{L}_{IM} into our framework.

4.4. Further Analysis

Parameter Analysis. The proposed method includes two parameters in MULT, i.e., α in Eq.10 and β in Eq.13. To investigate the impact of these two parameters, we varied their values, as depicted in Figure 3. We find when $0.15 \leq \alpha \leq 0.3$ and $0.6 \leq \beta \leq 0.7$, the model achieves relatively outstanding performance. We set $\alpha = 0.2$ and $\beta = 0.7$ based on the experiments.

Pseudo-label Accuracy Analysis. To quantify the quality of the pseudo-labels, we calculate the accuracy of posi-

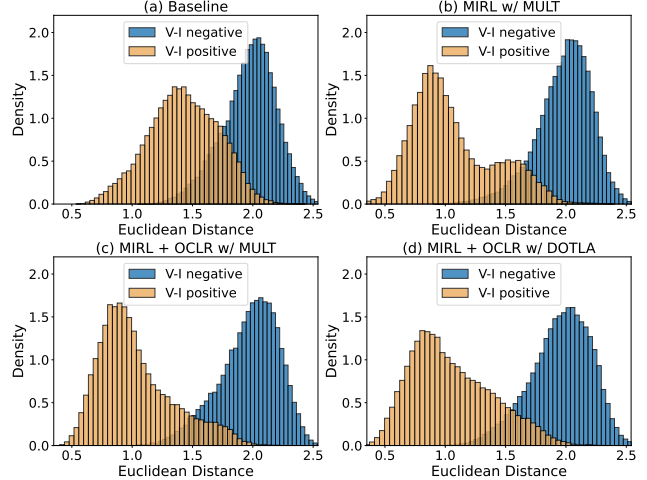


Figure 5. The visualization of distance distribution of randomly selected cross-modality positive and negative pairs.

tive instance pairs found by the pseudo-labels during training, as shown in Fig.4. We compare our MULT with DOTLA [6], and the results demonstrate that our MULT significantly facilitates the quality of pseudo labels. Simultaneously, the results indicate that as MULT and network training alternate, the network can continuously correct erroneous pseudo-labels.

Visualization. We visualize the Euclidean distance distribution of randomly selected 50000 positive and negative visible-infrared pairs, as shown in Fig.5. By sequentially integrating the modules (i.e., MULT, MIRL, and OCLR) into the training framework, we observe a convergence of cross-modality positive pairs and a divergence of negative pairs, demonstrating the effectiveness of each component in our framework to address the modality discrepancy. Fig.5 (c) and Fig.5 (d) further illustrate the superiority of MULT in comparison with DOTLA [6].

5. Conclusion

In this paper, we propose the Modality-Unified Label Transfer module to establish high-quality cross-modality pseudo-label associations for training. Our MULT lays emphasis on both homogeneous and heterogeneous context structure consistency by instance-wise affinities-guided label transfer. Furthermore, we introduce a straightforward yet effective plug-and-play Online Cross-memory Label Refinement module, which simultaneously mitigates the impact of noisy labels and facilitates modality alignment. Extensive experiments have demonstrated that our framework outperforms prior state-of-the-art methods.

Limitation. One major limitation of this study is there are still inevitable noisy labels from MULT and there is considerable potential for improvement in comparison to the supervised VI-ReID methods. In the future, we will investigate more robust cross-modality label association methods.

References

- [1] Mathilde Caron, Hugo Touvron, Ishan Misra, Hervé Jégou, Julien Mairal, Piotr Bojanowski, and Armand Joulin. Emerging properties in self-supervised vision transformers. In *Proceedings of the IEEE/CVF international conference on computer vision*, pages 9650–9660, 2021. 6
- [2] Dapeng Chen, Dan Xu, Hongsheng Li, Nicu Sebe, and Xiaogang Wang. Group consistent similarity learning via deep crf for person re-identification. In *Proceedings of the IEEE conference on computer vision and pattern recognition*, pages 8649–8658, 2018. 2
- [3] Hao Chen, Benoit Lagadec, and Francois Bremond. Ice: Inter-instance contrastive encoding for unsupervised person re-identification. In *Proceedings of the IEEE/CVF International Conference on Computer Vision*, pages 14960–14969, 2021. 6
- [4] Zhong Chen, Zhizhong Zhang, Xin Tan, Yanyun Qu, and Yuan Xie. Unveiling the power of clip in unsupervised visible-infrared person re-identification. In *Proceedings of the 31st ACM International Conference on Multimedia*, page 3667–3675, New York, NY, USA, 2023. Association for Computing Machinery. 6
- [5] De Cheng, Lingfeng He, Nannan Wang, Shizhou Zhang, Zhen Wang, and Xinbo Gao. Efficient bilateral cross-modality cluster matching for unsupervised visible-infrared person reid. In *Proceedings of the 31st ACM International Conference on Multimedia*, pages 1325–1333, 2023. 1, 2, 3, 5, 6, 7, 8
- [6] De Cheng, Xiaojian Huang, Nannan Wang, Lingfeng He, Zhihui Li, and Xinbo Gao. Unsupervised visible-infrared person reid by collaborative learning with neighbor-guided label refinement, 2023. 1, 2, 4, 6, 7, 8
- [7] De Cheng, Xiaolong Wang, Nannan Wang, Zhen Wang, Xiaoyu Wang, and Xinbo Gao. Cross-modality person re-identification with memory-based contrastive embedding. *Proceedings of the AAAI Conference on Artificial Intelligence*, 37(1):425–432, 2023. 5
- [8] Yoonki Cho, Woo Jae Kim, Seunghoon Hong, and Sung-Eui Yoon. Part-based pseudo label refinement for unsupervised person re-identification. In *Proceedings of the IEEE/CVF Conference on Computer Vision and Pattern Recognition*, pages 7308–7318, 2022. 1, 2, 6
- [9] Nicolas Courty, Rémi Flamary, Devis Tuia, and Alain Rakotomamonjy. Optimal transport for domain adaptation, 2016. 4
- [10] Marco Cuturi. Sinkhorn distances: Lightspeed computation of optimal transportation distances, 2013. 4
- [11] Zuozhuo Dai, Guangyuan Wang, Weihao Yuan, Xiaoli Liu, Siyu Zhu, and Ping Tan. Cluster contrast for unsupervised person re-identification, 2023. 1, 2, 3, 5, 6
- [12] Jia Deng, Wei Dong, Richard Socher, Li-Jia Li, Kai Li, and Li Fei-Fei. Imagenet: A large-scale hierarchical image database. In *2009 IEEE conference on computer vision and pattern recognition*, pages 248–255. Ieee, 2009. 6
- [13] Martin Ester, Hans-Peter Kriegel, Jörg Sander, Xiaowei Xu, et al. A density-based algorithm for discovering clusters in large spatial databases with noise. In *kdd*, pages 226–231, 1996. 3
- [14] Yixiao Ge, Dapeng Chen, and Hongsheng Li. Mutual mean-teaching: Pseudo label refinery for unsupervised domain adaptation on person re-identification. In *International Conference on Learning Representations*, 2020. 2, 6
- [15] Yixiao Ge, Feng Zhu, Dapeng Chen, Rui Zhao, et al. Self-paced contrastive learning with hybrid memory for domain adaptive object re-id. *Advances in neural information processing systems*, 33:11309–11321, 2020. 2, 3, 5
- [16] Yi Hao, Nannan Wang, Jie Li, and Xinbo Gao. Hsme: Hypersphere manifold embedding for visible thermal person re-identification. In *Proceedings of the AAAI conference on artificial intelligence*, pages 8385–8392, 2019. 1
- [17] Kaiping He, Xiangyu Zhang, Shaoqing Ren, and Jian Sun. Deep residual learning for image recognition. In *Proceedings of the IEEE conference on computer vision and pattern recognition*, pages 770–778, 2016. 3, 6
- [18] Kaiping He, Haoqi Fan, Yuxin Wu, Saining Xie, and Ross Girshick. Momentum contrast for unsupervised visual representation learning. In *Proceedings of the IEEE/CVF conference on computer vision and pattern recognition*, pages 9729–9738, 2020. 5
- [19] Mengxi Jia, Yunpeng Zhai, Shijian Lu, Siwei Ma, and Jian Zhang. A similarity inference metric for rgb-infrared cross-modality person re-identification. *arXiv preprint arXiv:2007.01504*, 2020. 1
- [20] Minsu Kim, Seungryong Kim, Jungin Park, Seongheon Park, and Kwanghoon Sohn. Partmix: Regularization strategy to learn part discovery for visible-infrared person re-identification. In *Proceedings of the IEEE/CVF Conference on Computer Vision and Pattern Recognition (CVPR)*, pages 18621–18632, 2023. 6
- [21] Thomas N Kipf and Max Welling. Semi-supervised classification with graph convolutional networks. *arXiv preprint arXiv:1609.02907*, 2016. 3
- [22] Mingkun Li, Chun-Guang Li, and Jun Guo. Cluster-guided asymmetric contrastive learning for unsupervised person re-identification. *IEEE Transactions on Image Processing*, 31: 3606–3617, 2022. 2
- [23] Xulin Li, Yan Lu, Bin Liu, Yating Liu, Guojun Yin, Qi Chu, Jinyang Huang, Feng Zhu, Rui Zhao, and Nenghai Yu. Counterfactual intervention feature transfer for visible-infrared person re-identification. In *European Conference on Computer Vision*, pages 381–398. Springer, 2022. 1, 2, 3, 6
- [24] Wenqi Liang, Guangcong Wang, Jianhuang Lai, and Xiaohua Xie. Homogeneous-to-heterogeneous: Unsupervised learning for rgb-infrared person re-identification. *IEEE Transactions on Image Processing*, 30:6392–6407, 2021. 2, 6, 7
- [25] Xinyu Lin, Jinxing Li, Zeyu Ma, Huafeng Li, Shuang Li, Kaixiong Xu, Guangming Lu, and David Zhang. Learning modal-invariant and temporal-memory for video-based visible-infrared person re-identification. In *Proceedings of the IEEE/CVF Conference on Computer Vision and Pattern Recognition*, pages 20973–20982, 2022. 1

- [26] Yutian Lin, Xuanyi Dong, Liang Zheng, Yan Yan, and Yi Yang. A bottom-up clustering approach to unsupervised person re-identification. In *Proceedings of the AAAI conference on artificial intelligence*, pages 8738–8745, 2019. [2](#)
- [27] Yutian Lin, Lingxi Xie, Yu Wu, Chenggang Yan, and Qi Tian. Unsupervised person re-identification via softened similarity learning. In *Proceedings of the IEEE/CVF conference on computer vision and pattern recognition*, pages 3390–3399, 2020. [2](#)
- [28] Jialun Liu, Yifan Sun, Feng Zhu, Hongbin Pei, Yi Yang, and Wenhui Li. Learning memory-augmented unidirectional metrics for cross-modality person re-identification. In *Proceedings of the IEEE/CVF Conference on Computer Vision and Pattern Recognition*, pages 19366–19375, 2022. [1](#), [6](#)
- [29] Yan Lu, Yue Wu, Bin Liu, Tianzhu Zhang, Baopu Li, Qi Chu, and Nenghai Yu. Cross-modality person re-identification with shared-specific feature transfer. In *Proceedings of the IEEE/CVF Conference on Computer Vision and Pattern Recognition (CVPR)*, 2020. [2](#), [3](#)
- [30] Chuanchen Luo, Yuntao Chen, Naiyan Wang, and Zhaoxiang Zhang. Spectral feature transformation for person re-identification. In *Proceedings of the IEEE/CVF international conference on computer vision*, pages 4976–4985, 2019. [2](#), [3](#)
- [31] Xudong Mao, Qing Li, and Haoran Xie. Aligngan: Learning to align cross-domain images with conditional generative adversarial networks, 2017. [1](#)
- [32] Islam Nassar, Munawar Hayat, Ehsan Abbasnejad, Hamid Reza Tofighi, and Gholamreza Haffari. Protocon: Pseudo-label refinement via online clustering and prototypical consistency for efficient semi-supervised learning. In *Proceedings of the IEEE/CVF Conference on Computer Vision and Pattern Recognition (CVPR)*, pages 11641–11650, 2023. [6](#)
- [33] Dat Tien Nguyen, Hyung Gil Hong, Ki Wan Kim, and Kang Ryoung Park. Person recognition system based on a combination of body images from visible light and thermal cameras. *Sensors*, 17(3):605, 2017. [6](#)
- [34] Zhiqi Pang, Chunyu Wang, Lingling Zhao, Yang Liu, and Gaurav Sharma. Cross-modality hierarchical clustering and refinement for unsupervised visible-infrared person re-identification. *IEEE Transactions on Circuits and Systems for Video Technology*, pages 1–1, 2023. [6](#)
- [35] Nan Pu, Wei Chen, Yu Liu, Erwin M Bakker, and Michael S Lew. Dual gaussian-based variational subspace disentanglement for visible-infrared person re-identification. In *Proceedings of the 28th ACM International Conference on Multimedia*, pages 2149–2158, 2020. [1](#)
- [36] Yantao Shen, Hongsheng Li, Tong Xiao, Shuai Yi, Dapeng Chen, and Xiaogang Wang. Deep group-shuffling random walk for person re-identification, 2018. [2](#)
- [37] Yantao Shen, Hongsheng Li, Shuai Yi, Dapeng Chen, and Xiaogang Wang. Person re-identification with deep similarity-guided graph neural network. In *Proceedings of the European conference on computer vision (ECCV)*, pages 486–504, 2018. [2](#)
- [38] Lei Tan, Yukang Zhang, Shengmei Shen, Yan Wang, Pingyang Dai, Xianming Lin, Yongjian Wu, and Rongrong Ji. Exploring invariant representation for visible-infrared person re-identification, 2023. [7](#)
- [39] Antti Tarvainen and Harri Valpola. Mean teachers are better role models: Weight-averaged consistency targets improve semi-supervised deep learning results. *Advances in neural information processing systems*, 30, 2017. [2](#)
- [40] Xudong Tian, Zhizhong Zhang, Shaohui Lin, Yanyun Qu, Yuan Xie, and Lizhuang Ma. Farewell to mutual information: Variational distillation for cross-modal person re-identification. In *Proceedings of the IEEE/CVF Conference on Computer Vision and Pattern Recognition*, pages 1522–1531, 2021. [6](#), [7](#)
- [41] Dongkai Wang and Shiliang Zhang. Unsupervised person re-identification via multi-label classification. In *Proceedings of the IEEE/CVF conference on computer vision and pattern recognition*, pages 10981–10990, 2020. [2](#)
- [42] Jiangming Wang, Zhizhong Zhang, Mingang Chen, Yi Zhang, Cong Wang, Bin Sheng, Yanyun Qu, and Yuan Xie. Optimal transport for label-efficient visible-infrared person re-identification. In *European Conference on Computer Vision*, pages 93–109. Springer, 2022. [1](#), [2](#), [4](#), [6](#), [7](#)
- [43] Menglin Wang, Baisheng Lai, Jianqiang Huang, Xiaojin Gong, and Xian-Sheng Hua. Camera-aware proxies for unsupervised person re-identification. In *Proceedings of the AAAI conference on artificial intelligence*, pages 2764–2772, 2021. [2](#)
- [44] Ancong Wu, Wei-Shi Zheng, Hong-Xing Yu, Shaogang Gong, and Jianhuang Lai. Rgb-infrared cross-modality person re-identification. In *Proceedings of the IEEE international conference on computer vision*, pages 5380–5389, 2017. [1](#), [6](#)
- [45] Qiong Wu, Pingyang Dai, Jie Chen, Chia-Wen Lin, Yongjian Wu, Feiyue Huang, Bineng Zhong, and Rongrong Ji. Discover cross-modality nuances for visible-infrared person re-identification. In *Proceedings of the IEEE/CVF Conference on Computer Vision and Pattern Recognition (CVPR)*, pages 4330–4339, 2021. [6](#)
- [46] Zesen Wu and Mang Ye. Unsupervised visible-infrared person re-identification via progressive graph matching and alternate learning. In *Proceedings of the IEEE/CVF Conference on Computer Vision and Pattern Recognition*, pages 9548–9558, 2023. [1](#), [2](#), [3](#), [6](#), [7](#), [8](#)
- [47] Bin Yang, Mang Ye, Jun Chen, and Zesen Wu. Augmented dual-contrastive aggregation learning for unsupervised visible-infrared person re-identification. In *Proceedings of the 30th ACM International Conference on Multimedia*, page 2843–2851, New York, NY, USA, 2022. Association for Computing Machinery. [2](#), [3](#), [5](#), [6](#), [7](#)
- [48] Bin Yang, Jun Chen, and Mang Ye. Towards grand unified representation learning for unsupervised visible-infrared person re-identification. In *Proceedings of the IEEE/CVF International Conference on Computer Vision (ICCV)*, pages 11069–11079, 2023. [2](#), [6](#), [7](#)
- [49] Mang Ye, Jianbing Shen, David J. Crandall, Ling Shao, and Jiebo Luo. Dynamic dual-attentive aggregation learning for visible-infrared person re-identification. In *Computer Vision—ECCV 2020: 16th European Conference, Glasgow*,

UK, August 23–28, 2020, *Proceedings, Part XVII 16*, pages 229–247. Springer, 2020. [1](#), [2](#), [6](#)

- [50] Mang Ye, Weijian Ruan, Bo Du, and Mike Zheng Shou. Channel augmented joint learning for visible-infrared recognition. In *Proceedings of the IEEE/CVF International Conference on Computer Vision*, pages 13567–13576, 2021.
- [51] Mang Ye, Jianbing Shen, Gaojie Lin, Tao Xiang, Ling Shao, and Steven C. H. Hoi. Deep learning for person re-identification: A survey and outlook, 2021. [1](#), [6](#)
- [52] Hong-Xing Yu, Wei-Shi Zheng, Ancong Wu, Xiaowei Guo, Shaogang Gong, and Jian-Huang Lai. Unsupervised person re-identification by soft multilabel learning. In *Proceedings of the IEEE/CVF conference on computer vision and pattern recognition*, pages 2148–2157, 2019. [2](#)
- [53] Guoqing Zhang, Hongwei Zhang, Weisi Lin, Arun Kumar Chandran, and Xuan Jing. Camera contrast learning for unsupervised person re-identification. *IEEE Transactions on Circuits and Systems for Video Technology*, 2023. [2](#)
- [54] Xiao Zhang, Yixiao Ge, Yu Qiao, and Hongsheng Li. Refining pseudo labels with clustering consensus over generations for unsupervised object re-identification. In *Proceedings of the IEEE/CVF Conference on Computer Vision and Pattern Recognition*, pages 3436–3445, 2021. [2](#)
- [55] Xinyu Zhang, Dongdong Li, Zhigang Wang, Jian Wang, Er-rui Ding, Javen Qinfeng Shi, Zhaoxiang Zhang, and Jingdong Wang. Implicit sample extension for unsupervised person re-identification. In *Proceedings of the IEEE/CVF Conference on Computer Vision and Pattern Recognition*, pages 7369–7378, 2022. [1](#), [2](#), [3](#)
- [56] Yukang Zhang, Yan Yan, Yang Lu, and Hanzi Wang. Towards a unified middle modality learning for visible-infrared person re-identification. In *Proceedings of the 29th ACM International Conference on Multimedia*, pages 788–796, 2021. [1](#)
- [57] Zhun Zhong, Liang Zheng, Donglin Cao, and Shaozi Li. Re-ranking person re-identification with k-reciprocal encoding. In *Proceedings of the IEEE conference on computer vision and pattern recognition*, pages 1318–1327, 2017. [4](#), [7](#)
- [58] Dengyong Zhou, Olivier Bousquet, Thomas Lal, Jason Weston, and Bernhard Schölkopf. Learning with local and global consistency. *Advances in neural information processing systems*, 16, 2003. [5](#)